Available online at www.sciencedirect.com
SCIENCE DIRECT®
ELSEVIER
European Journal of Mechanics B/Fluids 25 (2006) 192–203
EUROPEAN JOURNAL OF MECHANICS B/FLUIDS

Fluid stirrings in a circular cavity with various driven boundaries

Tzong-Yih Hwu *

Department of Computer Application Engineering, LanYang Institute of Technology, No 79, FuShin Rd., TouCheng, I-Lan Hsien, Taiwan 261

Received 30 November 2004; received in revised form 24 May 2005; accepted 7 July 2005

Available online 2 November 2005

Abstract

The present study deals with the complicated phenomena of fluid stirrings for the Stokes flows in a circular cavity. Two belts set on the boundary and periodically rotated with varied speeds construct the model flows. By means of the manipulations, the chaotic fluid stirrings prevail. Rather than to compute the finite-Lyapunov exponent in a local sense, a large number of fluid filaments are traced to quantitatively evaluate the averaged fluid stretch-rates in the cavity. Based on the results, several figures are provided to pre-estimate the overall fluid quantities that will be yielded when the installations and the rotations of the belts are specified. In general, the belts counter-rotated out of phase with longer periods are beneficial to the fluid stirrings. On the other hand, the variations of the fluid stretches with the belt installations are ambiguous. The maximum of the averaged fluid stretch-rates is about of 960 and 1.6 for the minimum.

Keywords: Fluid stirring; Stokes flow; Circular cavity; Averaged fluid stretch-rate

1. Introduction

In the last two decades, phenomena of fluid stirrings generated by chaotic advections of the Stokes flows have been extensively investigated. The manner in which chaotic fluid particle trajectories perform mechanical fluid mixing can be understood from the point of view of dynamical systems. When fluids move in two dimensions, the two equations for the velocity components constitute a dynamical system with the stream-function as the Hamiltonian. The two space co-ordinates are the familiar generalized co-ordinate and the generalized momentum, respectively. When the flow is in a steady state, the dynamical system is integrable because it has only one degree of freedom. The resulting fluid particle trajectories are regular and predictable, with no opportunity for random motions.

Sometimes however, chaotic flow motions are desired, for example in processes of fluid stirrings. Such stirrings can be easily achieved by subjecting flows to some time-periodic boundary conditions. Because the additional $1/2$ degree of freedom, time, is introduced into the dynamical system, the integrability of steady flows is destroyed. In that situation, some parts, or even all, of the fluid experience random motions and the fluid materials are redistributed uniformly. Besides being interesting in its own right, the phenomenon of fluid stirrings by Stokes flows has many

* Mailing address: 2F, No 7, Alley 38, Lane 31, Yu-Ying Street, Wen-Shan District, Taipei 116, Taiwan. Tel.: +886-3-9771997ext 260; fax: +886-2-29303414.

E-mail address: tyhwu@mail.fit.edu.tw (T.-Y. Hwu).

0997-7546/$ – see front matter
doi:10.1016/j.euromechflu.2005.07.003

industrial applications, for example, in material processing, in biochemical and biomedical processes, and in food engineering.

Two-dimensional flows with chaotic fluid stirrings may be obtained, first, in a journal bearing configuration. The apparatus consists of two cylinders for which one is put eccentrically within the other and fluid is filled throughout the gap in-between the cylinders. One periodically rotates the cylinders to perform fluid mixing. Aref and Balachandar [1] studied the kinematical features of the flows to conclude that boundaries moving with longer periods will yield better fluid stirrings. Chaiken et al. [2] investigated the flow motions in their experiments and captured two significant flow structures. One is a whorl and the other a tendril that were named by Berry et al. [3]. Swanson and Ottino [4] also performed a comprehensive study dealing with these flows. Their results obtained by experiments and computations compare favorably with each other. Dutta and Chevray [5] further explored the effects of molecular diffusions in the fluid stirrings to assert that, diffusion is enhanced when the interfacial areas between the fluid materials increase.

Chien, Rising, and Ottino [6] investigated the fluid stirrings in a rectangular cavity. They pointed out that the stirring efficiencies sensitively depend on the periods of the oscillations of the walls. As a time interval within which fluid is stirred is specified, there exists an optimal period with which the fluid would be stirred to create the highest efficiency. Leong and Ottino [7] experimentally studied the fluid stirrings to reveal several complicated phenomena including the birth, bifurcation and collapse of regular islands. Liu et al. [8] contend that (i) the regular island formulations, (ii) the corners of the boundaries and (iii) the unstable manifolds due to periodic hyperbolic points, will significantly influence the behaviors of the chaotic fluid stirrings.

Fluid motions in a circular cavity have been less studied than those in a rectangular cavity, even though the two flow patterns have geometric similarities. Tychonov and Samarski [9] have provided an analytical solution to the bi-harmonic equation for a circular domain. The solution in a closed form can readily be applied to the Stokes flows in a circular cavity, where one encounters the equation with the stream-function as the unknown variable. Such analytical solutions provide a powerful tool for the theoretical study of chaotic fluid stirrings in the circular cavity. This advantage will be exploited in the present work. The same solutions obtained using the Green function may be referred to Garabedian [10]. Mills [11] also investigated this problem and extended the solutions to apply to the flow configurations with the very small Reynolds numbers. Hwu, Young and Chen [12] used a circular cavity to stir fluids, for which a pair of belts are symmetrically installed and periodically rotated on the boundaries. In these studies, only theoretical and numerical works were performed. Based on the results, comprehensive fluid stirrings can be achieved by counter-rotating the belts with longer periods. Furthermore, the processes of deformation of the fluid filaments were described in detail and the finite-time Lyapunov exponents were computed to demonstrate the large fluid stretchings. Hwu [13] further investigated the quantitative dependences of the averaged fluid stretch-rates (this is abbreviated to AFSR in the present study) on the periodic boundary conditions. Rather than to evaluate the Lyapunov exponents that are frequently used in the other studies, the computations of AFSRs are introduced to represent the over-all fluid stirrings. The results indicate that better fluid stirrings would be obtained by rotating the belts out of phase and/or with longer periods. Under these conditions, the numbers of the fluid filaments with various stretch-rates have a uniform distribution.

Even though a number of results have been obtained in previous studies of the circular cavity, only the fluid stirrings performed by the two belts installing symmetrically and spanning $1/4$-cycles for each one were considered. Therefore, the present investigation aims to extensively and systematically study the fluid stirrings in a circular cavity with a variety of boundary conditions. The two belts are set symmetrically and asymmetrically with various lengths and positions. This is the key aspect of the present investigation which has not been addressed in literature. Moreover, the belts were temporally rotated at the angular velocities of squared sinusoidal functions. In virtue of this, two belts can be rotated at the same or opposite directions, and with various periods, angle-phase-shifts. AFSRs are computed to identify the influences of the boundary conditions on the fluid stirrings. As asserted previously, the circular cavity flows provide a powerful model to theoretically study the fluid stirrings. The results provide, if possible, guidance for the design of fluid mixers including the selection of suitable belt arrangements to create desired AFSRs.

2. Mathematical model and solutions

Fig. 1 schematically shows a circular cavity of unit radius filled with a Newtonian, incompressible fluid. Two belts, having lengths θ_1 and $\theta_3 - \theta_2$, are installed and rotated on the boundary to drive the liquid system. As the fluid moves in the Stokes flow regime, the corresponding stream-function can be written (Hwu et al. [12])

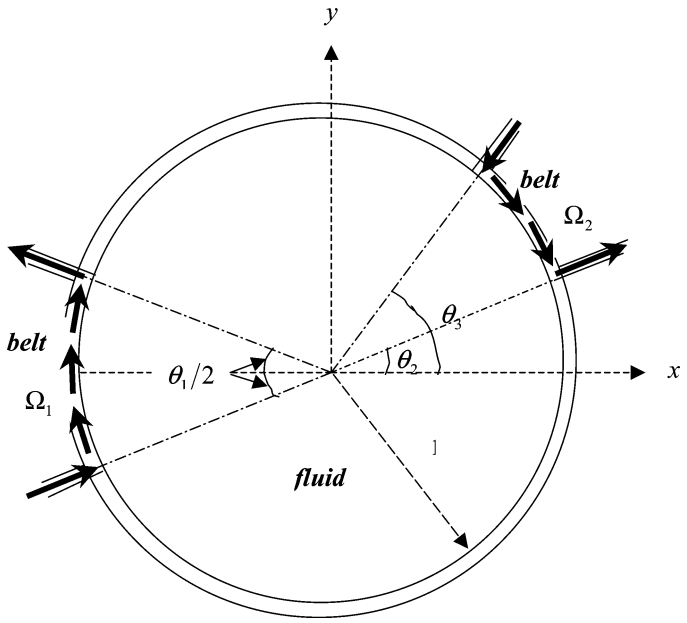

Fig. 1. Sketch of circular cavity with two co-rotating or counter-rotating belts.

$$\Psi = \frac{1-x^2-y^2}{2\pi}\Omega_1\left\{\pi - \tan^{-1}\left[\frac{(1+x^2+y^2+2x)\cot(\theta_1/4)+2y}{1-x^2-y^2}\right] - \tan^{-1}\left[\frac{(1+x^2+y^2+2x)\cot(\theta_1/4)-2y}{1-x^2-y^2}\right]\right\} + \frac{1-x^2-y^2}{2\pi}\Omega_2\left\{\tan^{-1}\left[\frac{(1+x^2+y^2+2x)\tan(\theta_3/2)-2y}{1-x^2-y^2}\right] - \tan^{-1}\left[\frac{(1+x^2+y^2+2x)\tan(\theta_2/2)-2y}{1-x^2-y^2}\right]\right\}. \quad (1)$$

This is obtained by the superposition of two flows, each obtained by rotating a single belt (Tychonov and Samarski [9], Garabedian [10], Mills [11]). In the above expression, Ω_1 and Ω_2 denote the rotating angular velocities of the belts. Next, the velocity fields of the circular cavity flows can be obtained by taking the derivatives of (1):

$$u = \frac{\mathrm{d}x}{\mathrm{d}t} = \frac{\partial \Psi}{\partial y} \quad \text{and} \quad v = \frac{\mathrm{d}y}{\mathrm{d}t} = -\frac{\partial \Psi}{\partial x}.$$

For performing chaotic fluid stirrings, the steady flow motions must be modulated. This can be achieved by rotating the belts at varied speeds. In the present study, the following protocols are adopted for the angular velocities of the rotating belts: $\Omega_1(t) = +2\sin^2(\pi t/T)$ and $\Omega_2(t) = \pm 2\sin^2(\pi t/T + \delta)$. T stands for the period of the time functions and δ for the angle-phase-shift. The positive sign in $\Omega_2(t)$ indicates co-rotations of the belts and the negative is for counter-rotations. It may be expected that the rotating angular velocities of the belts will play an important role in the chaotic fluid stirrings. Rather than directly solve the unsteady flow problems with the periodic boundary conditions, the cavity flows are further simplified for the mathematical analysis. It is required that the time scale of the momentum diffusion by the fluid molecular viscosity is much smaller than the period of rotation of the belts. Under the constraint, fluid is transported in a quasi-steady manner (Landau and Lifshitz [14]) and the velocities of the transient flows can be obtained by directly substituting $\Omega_1(t) = +2\sin^2(\pi t/T)$ and $\Omega_2(t) = \pm 2\sin^2(\pi t/T + \delta)$ into the expressions for the steady state. The resulting expressions for the velocities are lengthy and given in Appendix A.

To find fluid particle trajectories, one can then integrate (A.1) and (A.2) with respect to time. To deal with the complicated integrands, a Runge–Kutta scheme with accuracy of fourth order is used. The Poincaré sections are traditionally employed as a tool to globally detect the occurrences of the chaotic fluid motions. In the present work, such sections are obtained by simultaneously tracing twenty-eight fluid particles having the initial positions shown

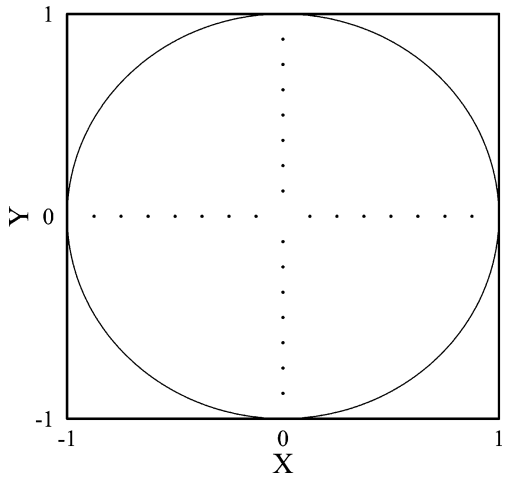

Fig. 2. Initial positions of 28 fluid tracers to generate the Poincaré sections for flows with various boundary conditions.

Table 1
Four steady flows in circular cavity with various boundary conditions

θ_1	θ_2	θ_3	Ω_1	Ω_2	Flow	Figure
0.5π	-0.5π	0	1	0.5	A	3(a)
				-0.5	B	3(b)
		0.5π	1	0.5	C	3(c)
				-0.5	D	3(d)

in Fig. 2. The successive positions of the fluid particles on one plane are then plotted for time equal to nT ($n = 1, 2, \ldots, 500$).

3. Results and discussion

Steady flows in the circular cavity are demonstrated first. Table 1 summarizes the parameters of four flows with various boundary conditions. In flow A and flow C, the belts are rotated in the same direction and the flow patterns are shown in Figs. 3(a) and 3(c), respectively. For each one of the flows, fluid moves in closed loops without separation. The flows with the pattern formation of a single bubble are preserved regardless of the value of Ω_1/Ω_2 and locations of the belts. On the other hand, flow B and flow D (Figs. 3(b) and 3(d)) both have counter-rotating belts yielding distinct fluid motions. In these two cases, a particular streamline exists which "splits" the flow domain into two parts. No fluid is permitted to transport through the interface between the two separated zones.

Before studying the time-dependent flows in the circular cavity, a convergence test of the numerical integrations can be performed to check that the correct fluid particle trajectories are obtained. This check is needed to guarantee that true physical chaos is encountered, where the fluid particles move in a random manner. A steady flow with co-rotated belts installed at $(\theta_1, \theta_2, \theta_3) = (\pi/2, -\pi/4, \pi/4)$ is examined. The total time interval for the computations is 500 and the Poincaré section is shown in Fig. 4. Because a fluid particle must be transported in a closed loop when it moves in a steady and closed flow, then the closed dotted curves demonstrate the accuracy of the numerical integrations for obtaining the trajectories.

For studying the main characteristics of the chaotic advections in the circular cavity, two flows with the belts installed at $(\theta_1 = \pi/2, \theta_2 = -\pi/2, \theta_3 = 0)$ and $(\theta_1 = \pi/2, \theta_2 = -\pi/2, \theta_3 = \pi/2)$ are treated. Both flows have the belts rotated out of phase, $\delta = \pi/2$. Fig. 5(a)–(c) illustrate the Poincaré sections generated by the flows for which the belts are installed at $(\theta_1 = \pi/2, \theta_2 = -\pi/2, \theta_3 = 0)$ and co-rotated with the periods of 1, 2, 3, respectively. Fig. 5(d)–(f) then exhibit the counter-rotating flows. Fig. 5(a) displays a re-circulating flow. Because the rotating angular velocities of the belts are varied with time, some points near the boundary undergo perturbed motion and spread. As the period increases up to $T = 2$, Fig. 5(b) shows that the regions of chaotic fluid motions grow to a

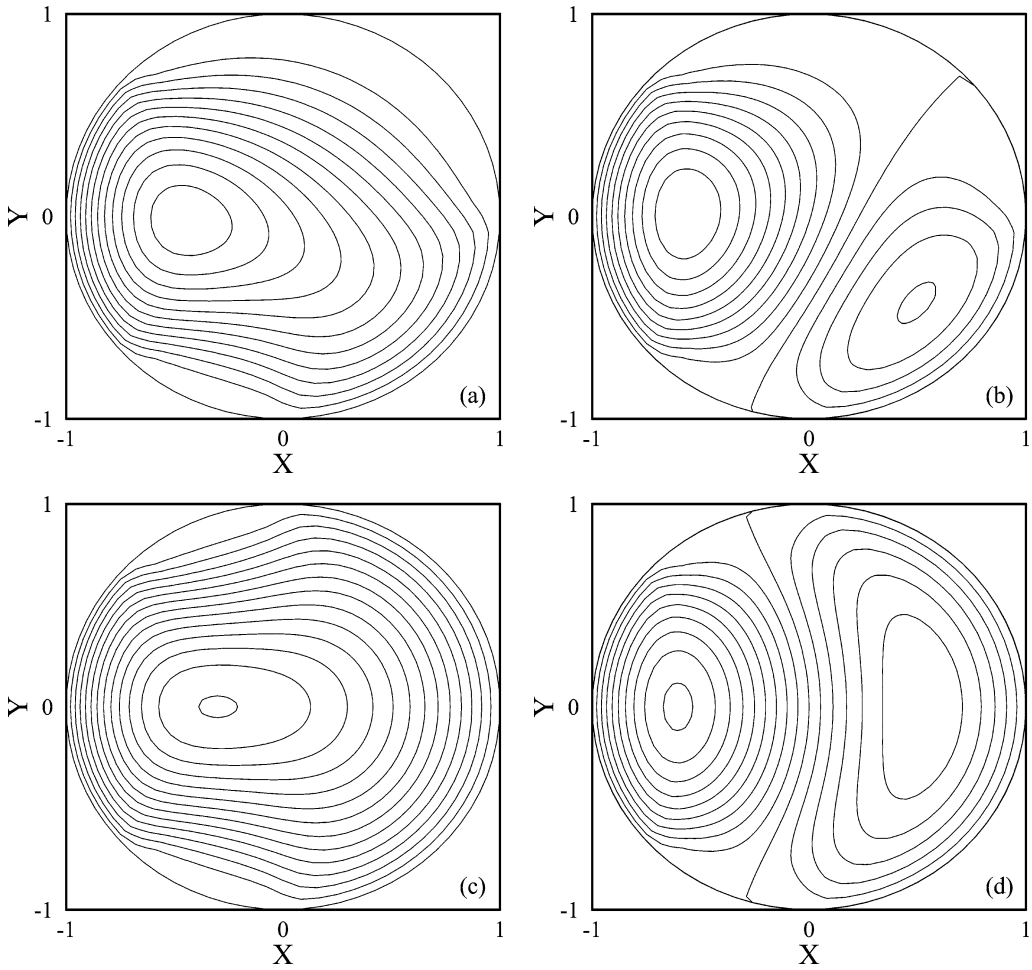

Fig. 3. Steady flow patterns with $\Delta\Psi = 0.02$. (a) Flow A: $\Psi_{\max} = 0.234$, $\Psi_{\min} = 0$; (b) Flow B: $\Psi_{\max} = 0.198$, $\Psi_{\min} = -0.082$; (c) Flow C: $\Psi_{\max} = 0.261$, $\Psi_{\min} = 0$; (d) Flow D: $\Psi_{\max} = 0.184$, $\Psi_{\min} = -0.117$.

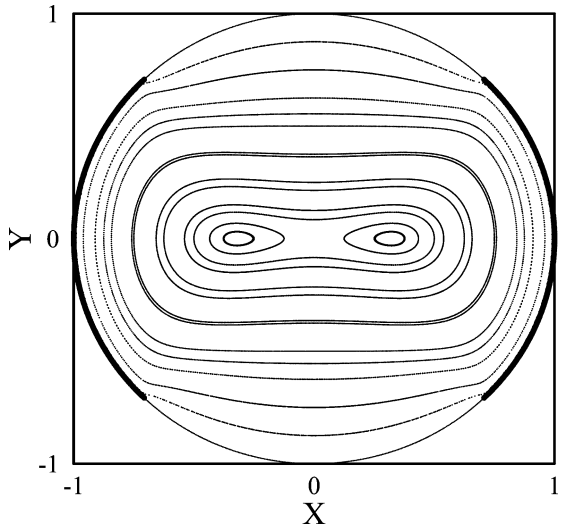

Fig. 4. Poincaré section of a steady flow with points located in closed loops to demonstrate the accuracy of the numerical integration of the particle trajectories.

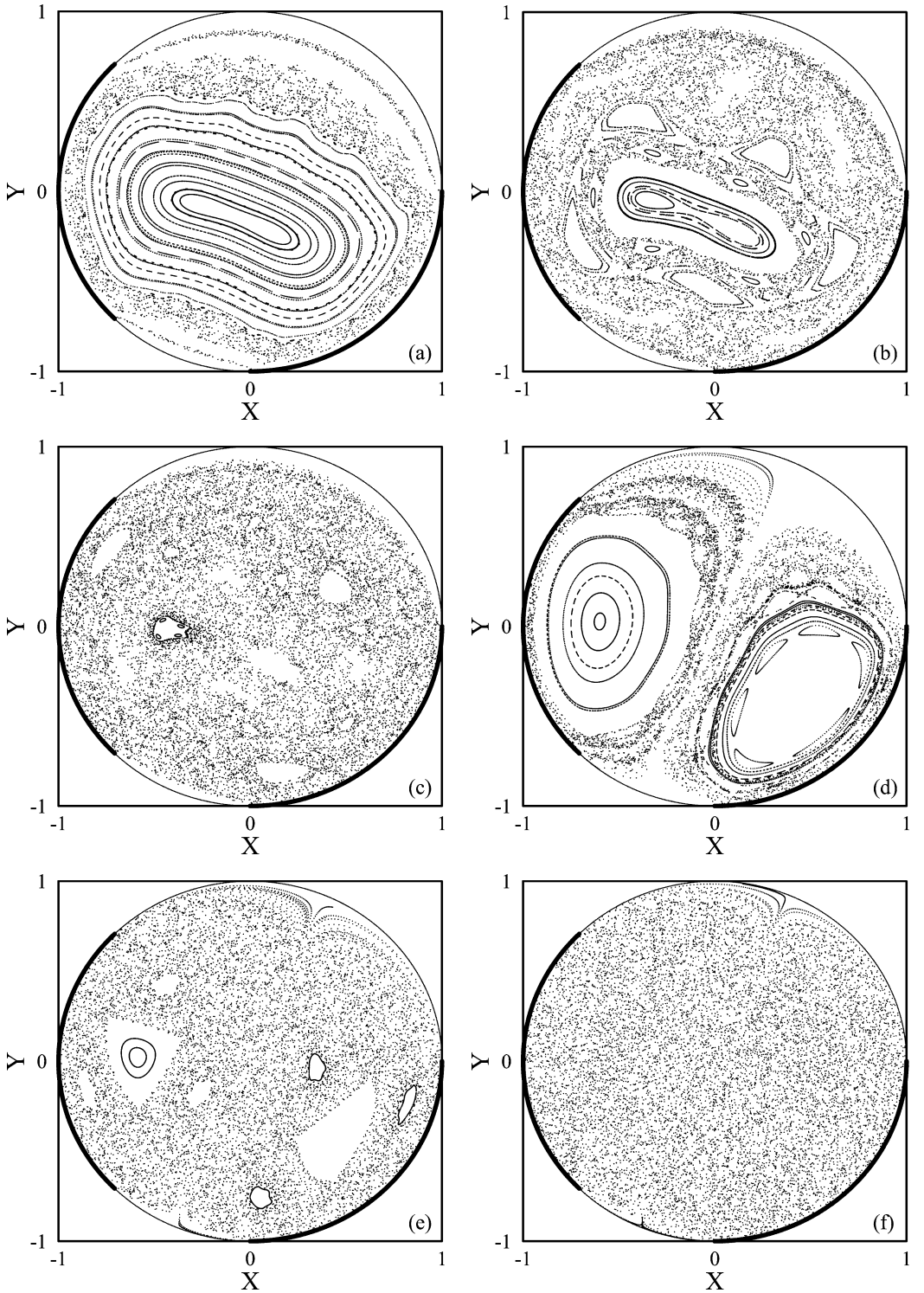

Fig. 5. Poincaré sections for flows with belts: $(\theta_1, \theta_2, \theta_3) = (\pi/2, -\pi/2, 0)$ and (a) co-rotations, period = 1, (b) co-rotations, period = 2, (c) co-rotations, period = 3, (d) counter-rotations, period = 1, (e) counter-rotations, period = 2, (f) counter-rotations, period = 3.

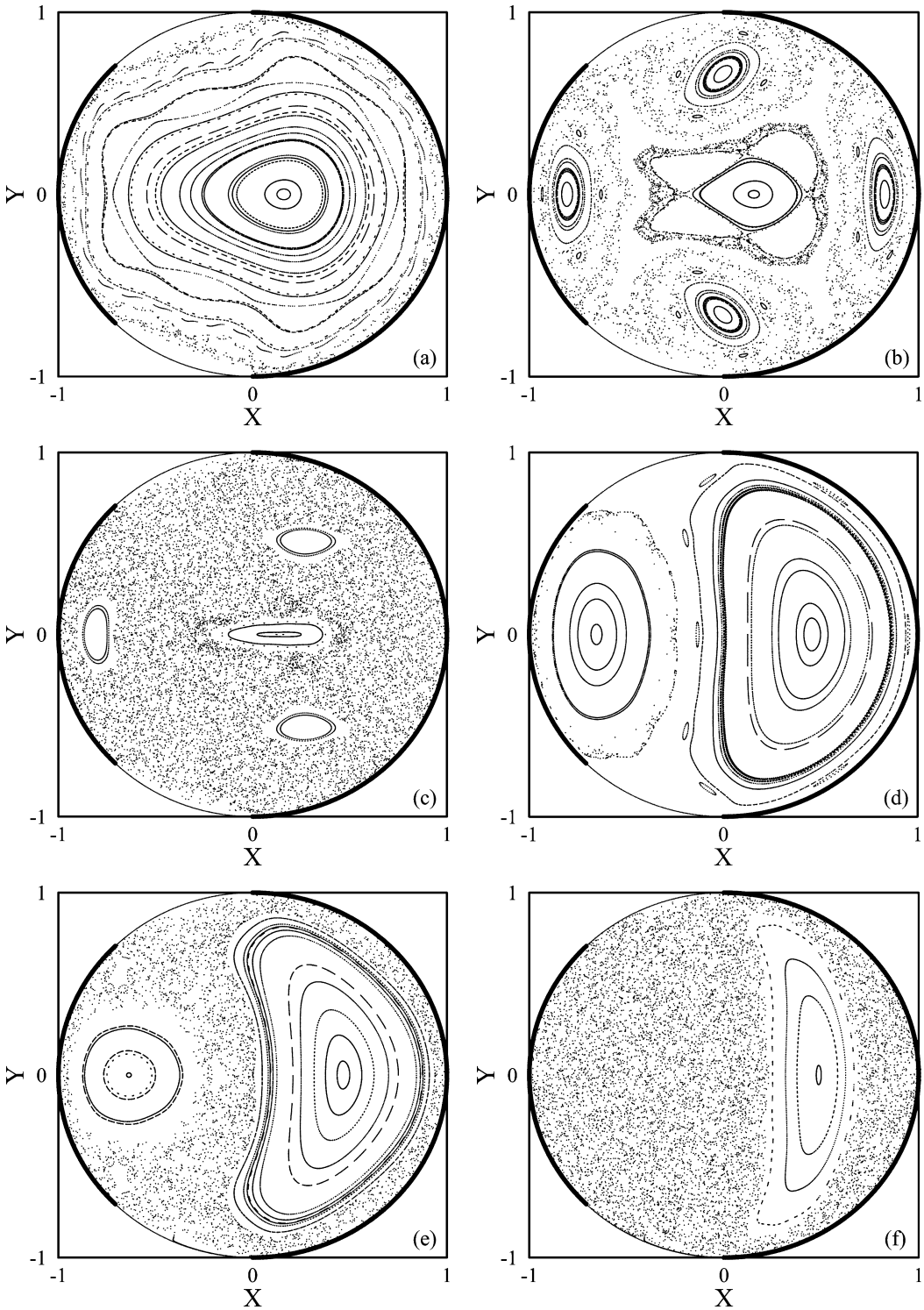

Fig. 6. Poincaré sections for flows with belts: $(\theta_1, \theta_2, \theta_3) = (\pi/2, -\pi/2, \pi/2)$ and (a) co-rotations, period = 1, (b) co-rotations, period = 2, (c) co-rotations, period = 3, (d) counter-rotations, period = 1, (e) counter-rotations, period = 2, (f) counter-rotations, period = 3.

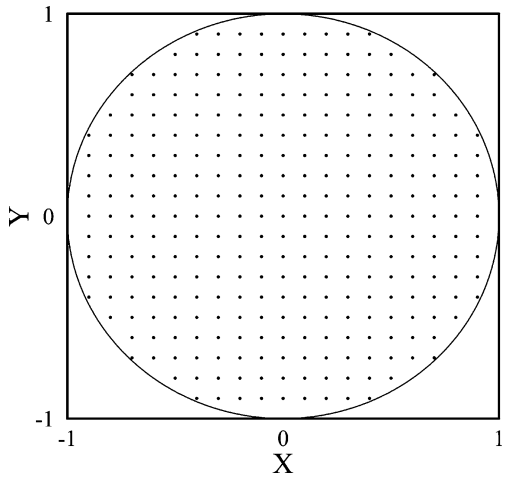

Fig. 7. Initial positions of 305 pairs of fluid filaments used to estimate averaged fluid stretch-rates.

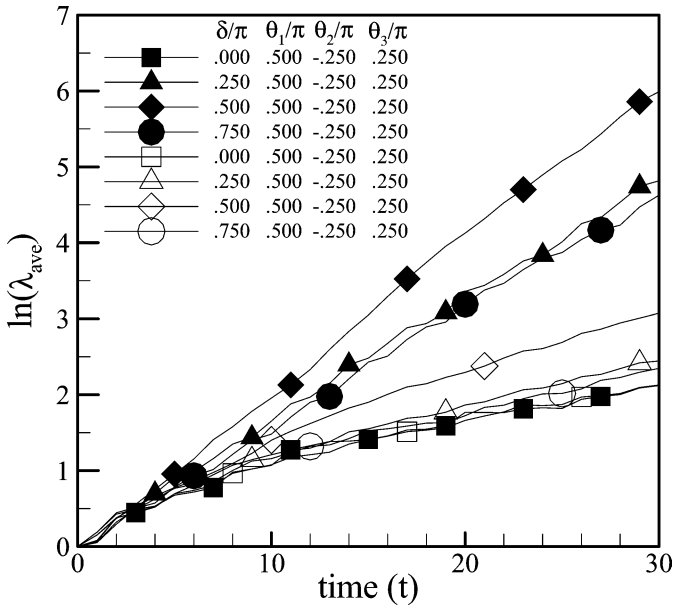

Fig. 8. Variations of AFSR-evolutions with δ (period = 3). Solid symbol: counter-rotation; Hollow symbol: co-rotation.

large extent, with regular fluid motions restricted to some big islands. It is interesting to notice that an island-chain of period-5 is captured. As the period increases up to $T = 3$ (Fig. 5(c)), a "chaos sea" occupies the entire cavity except for some small holes having negligible sizes. Fig. 5(d) shows the two-cell flow produced by the counter-rotating belts with $T = 1$. In the diagram, an island-chain of period-6 is clearly seen at the interface between the "white-hole", in which the fluid moves regularly, and the surrounding "chaos sea". This agrees with the prediction by the KAM theorem. As the period increases up to $T = 2$ (Fig. 5(e)), the regions within which the fluid moves in a regular way significantly decrease in sizes. As the period is further increased up to $T = 3$ (Fig. 5(f)), a uniform distribution of the points indicates the onset of complete fluid stirring. No matter whether the belts are counter-rotated or co-rotated, the fluid stirrings in the circular cavity seem to be enhanced by using longer periods.

The second flow, having the belt arrangement $\theta_1 = \pi/2, \theta_2 = -\pi/2, \theta_3 = \pi/2$, can now be discussed. Fig. 6(a) shows the Poincaré section obtained by co-rotating the belts with $T = 1$. A large sub-domain exists, within which the fluids are transported regularly to form closed loops. As the period increases up to $T = 2$ (Fig. 6(b)), the "chaos sea" grows and the regular fluid motions are confined to five isolated regions. As the period is further increased up to $T = 3$

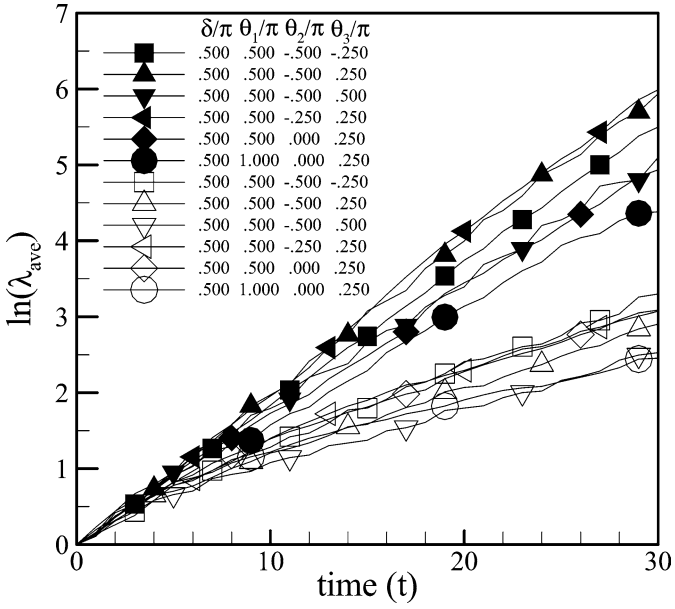

Fig. 9. Variations of AFSR-evolutions with belt installations (period = 3). Solid symbol: counter-rotation; Hollow symbol: co-rotation.

(Fig. 6(c)), most of the fluid undergoes chaotic advection. The corresponding results for the counter-rotating flows are illustrated in Fig. 6(d)–(f), respectively. Fig. 6(d) depicts an essentially regular flow pattern. As the period increases up to $T = 2$ (Fig. 6(e)), the "chaos sea" occupies some parts of the cavity and two islands of regular motions exist. As the period increases up to $T = 3$ (Fig. 6(f)), the "chaos sea" merges to leave only one big island within which the fluid moves in an orderly way. A comparison of Fig. 5(f) with Fig. 6(f) shows that the fluid stirrings are sensitive to where the belts are installed and what the belt lengths are, since both flows have the same protocols for the angular velocities of the rotating belts.

By comparing the figures we may conclude that chaotic flows in the circular cavity respond to the following features of the boundary conditions. The first feature is the rotation protocols of the belts, including period, angle-phase-shift, and direction; the second feature is the geometry of the belts, including position and length. The combination of these factors affects the fluid stirrings in a complicated, coupled manner. To characterize more precisely the dependence of the fluid stirrings on the boundary conditions, a quantity defined by $\lambda_{\text{ave}} \equiv \frac{1}{N}\sum_{i=1}^{N}(\lambda_{x,i} + \lambda_{y,i})/2$ (Hwu [13]) is computed in this study to represent the averaged fluid stretch-rate (AFSR) for the fluid throughout the entire cavity. In the expression, $\lambda \equiv l/l_0$ denotes the stretch-rate of a fluid filament that has the initial length l_0 and evolves to l as time proceeds. $\lambda_{x,i}$ and $\lambda_{y,i}$ stand for the stretch-rates of the ith pair of fluid filaments that join together initially and align with the orientations parallel to x-axis and y-axis, respectively. N denotes the total number of the pairs of the fluid filaments used to evaluate AFSR, λ_{ave}. In the following computations, the values of the parameters are chosen as $l_0 = 0.001$ and $N = 305$. Fig. 7 shows the initial positions of the 305 pairs of fluid filaments used for this propose.

Fig. 8 shows the dependence of the AFSRs on the angle-phase-shifts. Flows with the belts installed at ($\theta_1 = \pi/2, \theta_2 = -\pi/4, \theta_3 = \pi/4$) and with period = 3 are computed. The results shown in the diagram indicate that flows driven by counter-rotating belts have greater AFSRs than those driven by the co-rotating belts. Furthermore, rotating the belts out of phase, $\delta = \pi/2$, tends to increase the AFSRs. When the belts are rotated in phase, $\delta = 0$, the smallest AFSRs are induced no matter whether the boundaries are counter-rotated or co-rotated. Fig. 9 shows the variations of AFSRs with $(\theta_1, \theta_2, \theta_3)$. In these computations, the belts are rotated out of phase and with the period equal to 3. For the counter-rotated belts, the greatest AFSR is generated by the flow with ($\theta_1 = \pi/2, \theta_2 = -\pi/4, \theta_3 = \pi/4$) and the smallest by that with ($\theta_1 = \pi, \theta_2 = 0, \theta_3 = \pi/4$), respectively. On the other hand, the belts co-rotated and installed at ($\theta_1 = \pi/2, \theta_2 = -\pi/2, \theta_3 = -\pi/4$), ($\theta_1 = \pi/2, \theta_2 = -\pi/2, \theta_3 = \pi/2$) lead to the greatest and smallest AFSRs. Based on the results, AFSRs obtained by the counter-rotating belts are higher than those for co-rotating belts, no matter where the belts are installed. In addition, nearly identical AFSRs may be obtained for belts installed at

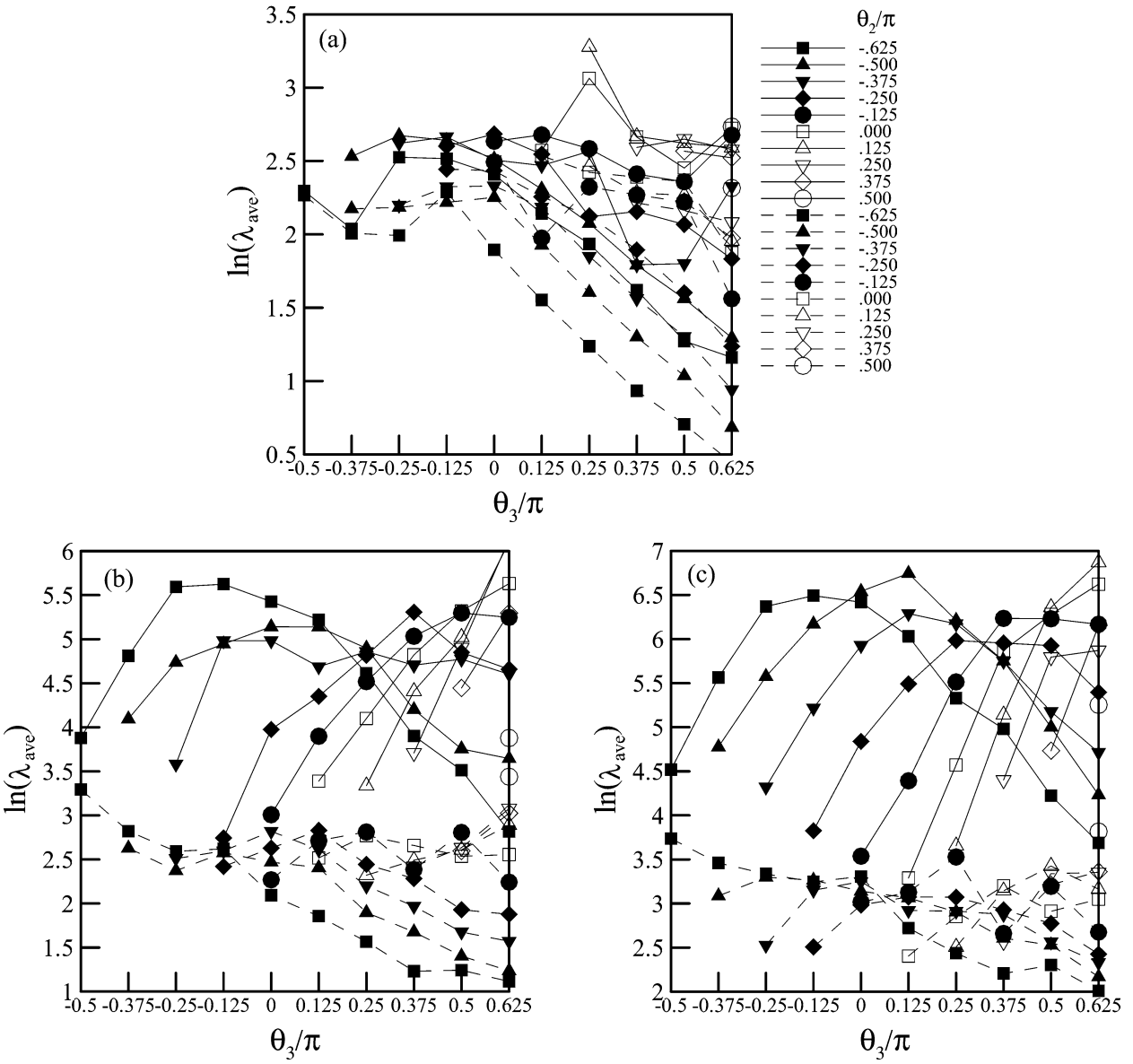

Fig. 10. AFSRs for flows with various belt installations ($\theta_1 = \pi/2$, period = 3). Solid line: counter-rotation; Dashed line: co-rotation. (a) $\delta = 0$, (b) $\delta = \pi/4$, (c) $\delta = \pi/2$.

Table 2
Extreme values of averaged fluid stretch-rates and corresponding belt installations (all flows obtained for $\theta_1 = \pi/2$ and $T = 3$)

Boundary conditions	δ	Maximum			Minimum			
Rotating type		λ_{ave}	(θ_2, θ_3)	length	λ_{ave}	(θ_2, θ_3)	length	
Counter-rotation	0	26.5	$\pi/8, \pi/4$	$\pi/8$	3.2	$-5\pi/8, 5\pi/8$	$5\pi/4$	Fig. 10(a)
Counter-rotation	$\pi/4$	460.4	$\pi/4, 5\pi/8$	$3\pi/8$	15.6	$-\pi/4, -\pi/8$	$\pi/8$	Fig. 10(b)
Counter-rotation	$\pi/2$	962.9	$\pi/8, 5\pi/8$	$\pi/2$	26.8	$0, \pi/8$	$\pi/8$	Fig. 10(c)
Counter-rotation	$3\pi/4$	410.5	$-5\pi/8, -\pi/8$	$\pi/2$	15.7	$-5\pi/8, 5\pi/8$	$5\pi/4$	
Co-rotation	0	12.6	$0, \pi/8$	$\pi/8$	1.6	$-5\pi/8, 5\pi/8$	$5\pi/4$	Fig. 10(a)
Co-rotation	$\pi/4$	31.1	$\pi/2, 5\pi/8$	$\pi/8$	3.1	$-5\pi/8, 5\pi/8$	$5\pi/4$	Fig. 10(b)
Co-rotation	$\pi/2$	45.4	$\pi/2, 5\pi/8$	$\pi/8$	7.5	$-5\pi/8, 5\pi/8$	$5\pi/4$	Fig. 10(c)
Co-rotation	$3\pi/4$	33.2	$-5\pi/8, -\pi/2$	$\pi/8$	3.4	$-\pi/2, 5\pi/8$	$9\pi/8$	

different positions. This is evidenced, for example, in the flows with $(\theta_1 = \pi/2, \theta_2 = 0, \theta_3 = \pi/4)$ and $(\theta_1 = \pi/2, \theta_2 = -\pi/2, \theta_3 = \pi/2)$.

Summarizing the results illustrated as above, AFSRs are sensitive to the boundary condition characteristics, including δ, T, rotating directions, θ_1, θ_2 and θ_3. The influences of the factors are difficult to separate from each other as they combine their effects. To address these difficulties, the following analyses will systematically estimate AFSRs of the circular cavity flows subject to a variety of boundary conditions. In the flows, one of the belts is given a fixed span $\theta_1 = \pi/2$ and the other spans sectors going from $\theta_2 = (n-6)\pi/8$ $(n = 1, 2, \ldots, 10)$ to $\theta_3 = \theta_2 + m(\pi/8) \leqslant 5\pi/8$ $(m = 1, 2, \ldots)$. Accordingly, there are 55 cavities of different boundary conditions to be computed. Moreover, the belts are either counter-rotated or co-rotated with the period set equal to 3. The angle-phase-shifts are chosen to be 0, $\pi/4$, $\pi/2$, $3\pi/4$, respectively, and all of AFSRs are evaluated at $t = 30$.

Fig. 10(a) illustrates AFSRs for $\delta = 0$. Due to the in-phase motion of the belts, the values of AFSRs are smaller than $e^{3.5} = 33.1$ for the counter-rotations and smaller than $e^{2.5} = 12.2$ for the co-rotations. Fig. 10(b) then shows the corresponding results for $\delta = \pi/4$. In these situations, AFSRs for the counter-rotations increase significantly compared with those for $\delta = 0$ and the values are obviously higher than those for co-rotations. In the plots of the counter-rotations, the curves designated with $\theta_2 = -5\pi/8, -\pi/2, -\pi/4$ have the form of a single peak. An optimization problem must be solved to choose the belt length which maximizes the AFSR, when the position of one end of the belt, θ_2, is specified. Fig. 10(c) shows AFSRs obtained by rotating the belts out of phase, $\delta = \pi/2$. Under these conditions, the values of AFSRs are higher than these for $\delta = 0$ and $\delta = \pi/4$. The variations of AFSRs for $\delta = 3\pi/4$ are similar to these for $\delta = \pi/4$ and are thus not plotted.

Table 2 summarizes the greatest and the smallest AFSRs created by the flows with the specified boundary conditions. The belt parameters (θ_2, θ_3) generating the extreme values are also given. Based on the results, the greatest AFSR with the magnitude of 960 occurs in the cavity flow by using the belts with the following conditions: counter-rotation, $\delta = \pi/2$, and $(\theta_2, \theta_3) = (\pi/8, 5\pi/8)$. The smallest AFSR with the magnitude of 1.6 occurs in the flow by using the belts with the following conditions: co-rotation, $\delta = 0$, and $(\theta_2, \theta_3) = (-5\pi/8, 5\pi/8)$. The dependence of the AFSRs on the belt geometry (positions and lengths) does not exhibit any clear trend.

4. Conclusions

The kinematical features of the chaotic advections and the averaged fluid stretch-rates for the Stokes flows in a circular cavity were investigated in the present study. Two belts installed on the boundary drive the fluid motions. A large number of computations with various boundary conditions were carried out to demonstrate in detail the variations of AFSRs. In general, the greater AFSRs are encountered in the circular cavity flows by counter-rotating the belts, out of phase, and with longer periods. The greatest AFSR of 960 is obtained by using belts counter-rotated out of phase and installed at $-\pi < \theta < -3\pi/4 \cup 3\pi/4 < \theta < \pi$, $\pi/8 < \theta < 5\pi/8$. The smallest AFSR of 1.6 is obtained by using the belts installed at $-\pi < \theta < -3\pi/4 \cup 3\pi/4 < \theta < \pi$, $-5\pi/8 < \theta < 5\pi/8$ and co-rotated in phase. Based on this study, several diagrams are provided which can be used to predict AFSRs in the circular cavity when the boundary conditions are specified.

Acknowledgements

This work is supported by the National Science Council of the Republic of China under Research Grants NSC 89-2211-E-267-001, NSC 90-2211-E-267-004 and NSC-91-2211-E-267-003.

Appendix A

The two velocity components of a fluid particle are expressed by

$$\frac{\mathrm{d}x}{\mathrm{d}t} = u = -\frac{y}{\pi} \cdot 2\sin^2\left(\frac{\pi t}{T}\right)\left\{\pi - \tan^{-1}\left[\frac{(1+x^2+y^2+2x)\cot(\theta_1/4)+2y}{1-x^2-y^2}\right] - \tan^{-1}\left[\frac{(1+x^2+y^2+2x)\cot(\theta_1/4)-2y}{1-x^2-y^2}\right]\right\} - \frac{1-x^2-y^2}{2\pi} \times 2\sin^2\left(\frac{\pi t}{T}\right)$$

$$\times\left\{\frac{(1-x^2-y^2)[2y\cot(\theta_1/4)+2]+2y(1+x^2+y^2+2x)\cot(\theta_1/4)+4y^2}{(1-x^2-y^2)^2+[(1+x^2+y^2+2x)\cot(\theta_1/4)+2y]^2}\right.$$
$$\left.+\frac{(1-x^2-y^2)[2y\cot(\theta_1/4)-2]+2y(1+x^2+y^2+2x)\cot(\theta_1/4)-4y^2}{(1-x^2-y^2)^2+[(1+x^2+y^2+2x)\cot(\theta_1/4)-2y]^2}\right\}$$
$$\mp\frac{y}{\pi}\cdot 2\sin^2\left(\frac{\pi t}{T}+\delta\right)\left\{\tan^{-1}\left[\frac{(1+x^2+y^2+2x)\tan(\theta_3/2)-2y}{1-x^2-y^2}\right]\right.$$
$$\left.-\tan^{-1}\left[\frac{(1+x^2+y^2+2x)\tan(\theta_2/2)-2y}{1-x^2-y^2}\right]\right\}\pm\frac{1-x^2-y^2}{2\pi}\times 2\sin^2\left(\frac{\pi t}{T}+\delta\right)$$
$$\times\left\{\frac{(1-x^2-y^2)[2y\tan(\theta_3/2)-2]+2y(1+x^2+y^2+2x)\tan(\theta_3/2)-4y^2}{(1-x^2-y^2)^2+[(1+x^2+y^2+2x)\tan(\theta_3/2)-2y]^2}\right.$$
$$\left.-\frac{(1-x^2-y^2)[2y\tan(\theta_2/2)-2]+2y(1+x^2+y^2+2x)\tan(\theta_2/2)-4y^2}{(1-x^2-y^2)^2+[(1+x^2+y^2+2x)\tan(\theta_2/2)-2y]^2}\right\} \tag{A.1}$$

and

$$\frac{\mathrm{d}y}{\mathrm{d}t}=v=\frac{x}{\pi}\cdot 2\sin^2\left(\frac{\pi t}{T}\right)\left\{\pi-\tan^{-1}\left[\frac{(1+x^2+y^2+2x)\cot(\theta_1/4)+2y}{1-x^2-y^2}\right]\right.$$
$$\left.-\tan^{-1}\left[\frac{(1+x^2+y^2+2x)\cot(\theta_1/4)-2y}{1-x^2-y^2}\right]\right\}+\frac{1-x^2-y^2}{2\pi}\times 2\sin^2\left(\frac{\pi t}{T}\right)$$
$$\times\left\{\frac{(1-x^2-y^2)(2x+2)\cot(\theta_1/4)+2x(1+x^2+y^2+2x)\cot(\theta_1/4)+4xy}{(1-x^2-y^2)^2+[(1+x^2+y^2+2x)\cot(\theta_1/4)+2y]^2}\right.$$
$$\left.+\frac{(1-x^2-y^2)(2x+2)\cot(\theta_1/4)+2x(1+x^2+y^2+2x)\cot(\theta_1/4)-4xy}{(1-x^2-y^2)^2+[(1+x^2+y^2+2x)\cot(\theta_1/4)-2y]^2}\right\}$$
$$\pm\frac{x}{\pi}\cdot 2\sin^2\left(\frac{\pi t}{T}+\delta\right)\left\{\tan^{-1}\left[\frac{(1+x^2+y^2+2x)\tan(\theta_3/2)-2y}{1-x^2-y^2}\right]\right.$$
$$\left.-\tan^{-1}\left[\frac{(1+x^2+y^2+2x)\tan(\theta_2/2)-2y}{1-x^2-y^2}\right]\right\}\mp\frac{1-x^2-y^2}{2\pi}\times 2\sin^2\left(\frac{\pi t}{T}+\delta\right)$$
$$\times\left\{\frac{(1-x^2-y^2)(2x+2)\tan(\theta_3/2)+2x(1+x^2+y^2+2x)\tan(\theta_3/2)-4xy}{(1-x^2-y^2)^2+[(1+x^2+y^2+2x)\tan(\theta_3/2)-2y]^2}\right.$$
$$\left.-\frac{(1-x^2-y^2)(2x+2)\tan(\theta_2/2)+2x(1+x^2+y^2+2x)\tan(\theta_2/2)-4xy}{(1-x^2-y^2)^2+[(1+x^2+y^2+2x)\tan(\theta_2/2)-2y]^2}\right\}. \tag{A.2}$$

References

[1] H. Aref, S. Balachandar, Chaotic advection in a Stokes flow, Phys. Fluids 29 (11) (1986) 3515–3521.
[2] J. Chaiken, R. Chevray, M. Tabor, Q.M. Tan, Experimental study of Lagrangian turbulence in a Stokes flow, Proc. Roy. Soc. London Ser. A 408 (1986) 165–174.
[3] M.V. Berry, N.L. Balazs, M. Tabor, A. Voros, Quantum maps, Ann. Phys. 122 (1979) 26–63.
[4] P.D. Swanson, J.M. Ottino, A comparative computational and experimental study of chaotic mixing of viscous fluids, J. Fluid Mech. 213 (1990) 227–249.
[5] P. Dutta, R. Chevray, Effect of diffusion on chaotic advection in Stokes flow, Phys. Fluids A 3 (5) (1991) 1440.
[6] W.L. Chien, H. Rising, J.M. Ottino, Laminar mixing and chaotic mixing in several cavity flows, J. Fluid Mech. 170 (1986) 355–377.
[7] C.W. Leong, J.M. Ottino, Experiments on mixing due to chaotic advection in a cavity, J. Fluid Mech. 209 (1989) 463–499.
[8] M. Liu, R.L. Peskin, F.J. Muzzio, C.W. Leong, Structure of the stretching field in chaotic cavity flows, AIChE J. 40 (8) (1994) 1273–1286.
[9] A.N. Tychonov, A.A. Samarski, Partial Differential Equation of Mathematical Physics 1, Holden-Day, San Francisco, 1964.
[10] P.R. Garabedian, Partial Differential Equations, John Wiley and Sons, New York, 1964.
[11] R.D. Mills, Computing internal viscous flow problem for the circle by integral method, J. Fluid Mech. 79 (3) (1977) 609–624.
[12] T.Y. Hwu, D.L. Young, Y.Y. Chen, Chaotic advections for Stokes flows in circular cavity, ASCE J. Engrg. Mech. 123 (8) (1997) 774–782.
[13] T.Y. Hwu, Stretches of fluid materials for Stokes flow in circular cavity, ASCE J. Engrg. Mech. 126 (5) (2000) 554–557.
[14] L.D. Landau, E.M. Lifshitz, Fluid Mechanics, Pergamon, Oxford, 1959.